

HydraWave: Multi-Group Multicast Hybrid Precoding and Low-Latency Scheduling for Ubiquitous Industry 4.0 mmWave Communications

Luis F. Abanto-Leon, Matthias Hollick, and Gek Hong (Allyson) Sim
Secure Mobile Networking (SEEMOO) Lab, Technische Universität Darmstadt, Germany
{labanto, mhollick, asim}@seemoo.tu-darmstadt.de

Abstract—Industry 4.0 anticipates massive interconnectivity of industrial devices (e.g., sensors, actuators) to support factory automation and production. Due to the rigidity of wired connections to harmonize with automation, wireless information transfer has attracted substantial attention. However, existing solutions for the manufacturing sector face critical issues in coping with the key performance demands: *ultra-low latency, high throughput, and high reliability*. Besides, recent advancements in wireless millimeter-wave (mmWave) technology advocates hybrid precoding with affordable hardware and outstanding spatial multiplexing performance. Thus, we present HYDRAWAVE — a new paradigm that contemplates the joint design of *group scheduling and hybrid precoding* for multi-group multicasting to support ubiquitous low-latency communications. Our flexible hybrid precoder, based on semidefinite relaxation and Cholesky matrix factorization, facilitates the robust design of the constant-modulus phase shifts rendering formidable performance at a fraction of the power required by fully-digital implementations. Further, our novel group scheduling formulation minimizes the number of scheduling windows while accounting for the channel correlation of the co-scheduled multicast receivers. Compared to exhaustive search, which renders the optimal scheduling at high overhead, HYDRAWAVE incurs only 9.5% more delay. Notoriously, HYDRAWAVE attains up to 102% gain when compared to the other benchmarked schemes.

Index Terms—hybrid precoding, multi-group multicasting, low-latency, Industry 4.0, millimeter-wave, scheduling.

I. INTRODUCTION

The industrial revolution, Industry 4.0, fosters smart factories of the future where the components in a production chain—such as industrial equipment, logistics, products, and processes—are inherently interconnected. Given the hyper-connected vision of Industry 4.0, wired connections become less attractive because they (i) hinder automation by constraining the movement of industrial robotics and (ii) slow down mechanics. To overcome this obstacle, in recent years, significant effort has been dedicated to leveraging the benefits of wireless communications solutions for the manufacturing sector (e.g., WirelessHART, 6TiSCH, ZigBee). However, the adoption of these technologies is either limited or has not been consolidated due to the uncertainty on their capability to offer performance similar to optical fiber and guarantee the critical requirements of industrial applications: *ultra-high throughput and ultra-low latency with emphasis on high reliability* [1].

Owing to recent advancements in wireless millimeter-wave (mmWave) technology, the mmWave spectrum is regarded as a solution to wire replacement in industrial/manufacturing sectors. In addition to providing multi-Gbps rates due to wideband availability, mmWave frequencies characterize for requiring

antennas with a small footprint that can be easily embedded onto miniature machinery/devices. A measurement campaign conducted in an industrial environment has concluded that mmWave communications is feasible and effortlessly implementable in such environments [2]. Nevertheless, the research on wireless and (in particular) mmWave technology for the industrial context is still at its infancy.

The industrial sectors can profoundly benefit from mmWave multicast beamforming to deliver common information to industrial equipment (e.g., sensors and actuators) for the distributed organization of production. In such setting, instead of sequentially transmitting unicast streams from a transmitter to each receiver (Fig. 1a), multicasting to a group of devices (Fig. 1b) can boost the spectral efficiency and offer lower latency. Moreover, if the transmitter is equipped with multiple radio frequency (RF) chains, multi-group multicasting can be enabled thus making possible to serve several groups of devices concurrently while further leveraging the gains in terms of spectral efficiency and latency (Fig. 1c).

We envision a heterogeneous hyper-connected Industry 4.0 with (i) *anchored receivers* (e.g., sensors, actuators, programmable logic devices) that perform tasks locally and (ii) *mobile receivers* (e.g., robots) that carry out tasks at various locations. Specifically, multiple *anchored receivers* from different multicast groups can be found sharing the same space, thus increasing the difficulty of spatial multiplexing (Fig. 1b). In addition, due to mobility (e.g. robots), numerous *mobile receivers* with different information needs may temporarily change their location to carry out specific tasks, thus either altering the density of devices at different phases of the production chain or generating a variable degree of interference.

Fully-digital precoders with a massive amount of antennas and RF chains are a tangible technology at sub-6GHz frequencies. However, in mmWave, these precoders are still not affordable due to hardware complexity and high power consumption. As a result, substantial effort has been oriented to (i) improve the architectures design (e.g., [3], [4]) and (ii) develop accurate channel estimation methods (e.g., [5], [6]) for hybrid precoders, aiming at facilitating physical-layer hybrid precoding with high signal-to-interference-plus-noise ratio (SINR). In industrial scenarios, the number of multicast groups is expected to be large in comparison to the number of RF chains, generating thereby the necessity for scheduling. Further, depending on how the groups are co-scheduled, the achievable performance of the precoder will be impacted. As a result, a scrupulous design that considers the joint

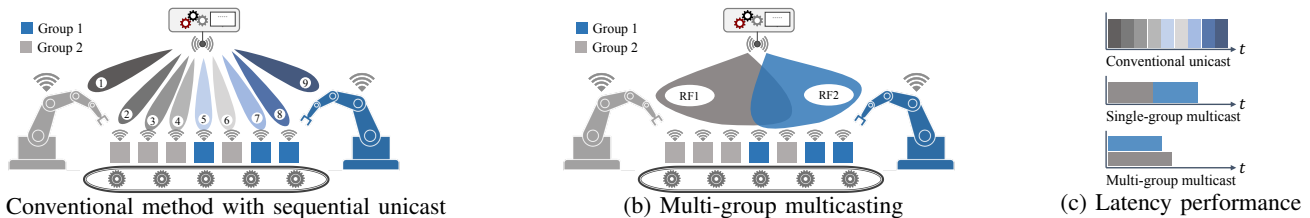


Figure 1: Comparison of mmWave unicast, conventional and proposed multi-group multicasting methods in Industry 4.0.

optimization of scheduling, hybrid precoder (at the transmitter) and analog combiners (at receivers) is required to comply with the requirements of industrial applications. To this end, we propose HYDRAWAVE, a versatile scheme that devises an *agile scheduler* and a *robust multi-group multicast precoder with analog combiners*, capable of providing *high throughput, low latency, and high reliability* (which is guaranteed through service ubiquitousness).

Table I: Literature on multicasting

Type	Scheduling with PHY abstraction	PHY design w/o scheduling		PHY design w/ scheduling	
		Fully-digital	Hybrid	Fully-digital	Hybrid
SGM	[7]–[9]	[10]–[14]	[12], [15]	[16], [17]	–
MGM	–	[18]–[25]	[26]–[28]	–	–

As shown in Table I, the literature on single-group multicasting (SGM) focus on either pure scheduling with physical-layer (PHY) abstraction [7]–[9] or physical-layer beamforming/precoding with [16], [17] and without scheduling [10]–[15], ignoring the interference aspect in multi-group multicast scenarios. On the other hand, the body of research on multi-group multicasting (MGM) focuses mostly on fully-digital precoder designs without scheduling tailored for sub-6GHz frequencies [18]–[25], which are not appropriate for mmWave. As a result, the more practical and cost-efficient hybrid precoders [26]–[28] have attracted substantial attention. Nevertheless, these solutions are either (i) constrained in application due to simplified assumptions [20], [27] or (ii) unimplementable in the existing multi-antenna hardware due to customized designs [26], [28]. Furthermore, the joint problem of *group scheduling* and *precoding* for multi-group multicasting has been studied for neither fully-digital nor hybrid precoders. The following summarizes our contributions:

- We introduce three propositions that support the design of precoders that ensure low-latency and high reliability. *Proposition 1* renders insights on the (approximate) inverse relation between SINR and latency. *Proposition 2* leverages on this result, and reveals that latency minimization is promoted when maximizing the minimum equalized SINR (e-SNR). This exposes a relevant relation with the max-min MGM problem. *Proposition 3* supports our formulation of optimal joint group scheduling and precoding for the multi-group multicast problem, with emphasis on latency minimization and high reliability.
- Due to the complexity of solving the problem related to *Proposition 3* (which requires exhaustive search), we devise a novel group scheduling formulation with a two-

fold objective: (i) minimizing the number of scheduling windows and (ii) reducing channel correlation between the co-scheduled receivers. To attain the latter objective, we introduce a metric called *aggregate inter-group correlation* that is shown to be highly suitable for forming the co-scheduled multicast groups. As a result, we only need to solve the problem associated with *Proposition 2* (which is comparatively simpler) for every window of the resultant scheduling thus reducing the complexity.

- The problem associated with *Proposition 2* is non-convex. Due to the NP-hardness of this problem, we propose an alternate optimization scheme where the analog and digital components of the hybrid precoder (at the transmitter), and the analog combiners (at each receiver) are optimized sequentially. We recast each sub-problem as a semidefinite relaxation (SDR) program in order to convexify the non-convex expressions.
- We propose a versatile approach based on Cholesky matrix factorization, capable of handling an arbitrary number of phase rotations at both the analog component of the hybrid precoder (at the transmitter) and the analog combiners (at the receivers) with outstanding performance.
- Compared to prior art on multi-group multicast precoding, we consider receivers with multiple antennas, which can be adopted at mmWave frequencies owing to the small antenna footprints.
- Through extensive simulations, we evaluate the performance of our hybrid precoder and compare it against fully-digital and fully-analog implementations. Further, we also assess our proposed HYDRAWAVE (joint group scheduling and precoding) and compare it in terms of *latency* against three competing approaches: single-group multicasting (SING), random scheduling (RAND) and exhaustive search (XHAUS). We show through simulations that HYDRAWAVE can attain gains up to 102% and 60% when compared against RAND and SING, respectively, while remaining within 9.5% optimality of XHAUS.

II. RELATED WORK

In SGM scheduling with physical-layer abstraction [7]–[9], the transmitter adjusts the gains of single-lobe switched beams to improve the SNR at the receivers. These works mainly focus on achieving high throughput with minimum delay for all the multicast receivers. Concerning SGM physical-layer precoding (hybrid/fully-digital and with/without scheduling), researchers have studied the quality-of-service (QoS) and max-min fairness problems [10]–[17]. Under these two categories, the QoS [18]–[22], [26], [27] and max-min fairness [21]–

[25], [28] problems have also been researched for the MGM case. Fully-digital precoders are highly versatile for interference mitigation due to the availability of numerous RF chains. However, these designs consumes excessive power and require expensive hardware (particularly for mmWave). To address these issues, the use of analog-digital architectures (i.e., hybrid precoders) have received considerable attention. Hybrid precoders are constituted by a low-dimensional digital precoder that allows interference management and a high-dimensional network of phase shifters, with an arbitrary set of phase rotations that facilitates beamsteering. These designs do not have the same versatility as fully-digital implementations but are more energy-efficient and practical. Nevertheless, the existing hybrid precoder solutions (in general, multicast and multi-user unicast designs) are restricted in usage due to either (i) simplified assumptions in phase rotations selection or (i) unimplementability owing to customized hardware. Specifically, the solution propounded in [28] requires a especially connected network of phase shifters for optimal operation. On the other hand, in [20], [27], the usage is constrained to only four different phase shifts. In [26], the analog phase shifters are replaced by high-resolution lens arrays with adjustable power, thus circumventing the actual problem of phase selection.

A work that focuses on a problem slightly related to ours is [29], where the authors study user selection and MGM precoding with fully-digital transmitters and single-antenna receivers. In [29], specific users for each multicast group are selected in order to maximize the sum-rate. Contrastingly, in our case we deal with group selection for which we devise a metric (i.e., IGC) that depicts the mean channel vector correlation among the receivers of each group. Also, in our case, the objective is to design the precoders aiming at the minimization of the transmission latency.

III. MULTI-GROUP MULTICAST SYSTEM MODEL

We consider a mmWave system where a next generation Node B (gNodeB) equipped with a hybrid precoder aims to schedule G_T multicast groups comprising a total of K_T receivers. The sets of receivers and groups are denoted by $\mathcal{K} = \{1, 2, \dots, K_T\}$ and $\mathcal{I} = \{1, 2, \dots, G_T\}$, respectively. In addition, \mathcal{G}_i represents the set of receivers in multicast group $i \in \mathcal{I}$. The number of receivers in the i -th multicast group is represented by $|\mathcal{G}_i|$. As in [21], we assume that $\mathcal{G}_i \cap \mathcal{G}_{i'} = \{\emptyset\}, \forall i \neq i'$. The hybrid precoder at the gNodeB exhibits a sub-connected architecture, which consists of N_{tx} transmit antennas and N_{tx}^{RF} RF chains. Thus, each RF chain is connected to a sub-array of $L_{tx} = N_{tx}/N_{tx}^{RF}$ antennas [3]. Due to capacity constraints, each receiver is equipped with purely analog combiners that consist of N_{rx} antennas and a single RF chain, i.e., $N_{rx}^{RF} = 1$ and $L_{rx} = N_{rx}$. Since, in general $G_T \geq N_{tx}^{RF}$, scheduling is necessary because N_{tx}^{RF} determines the maximum number of data streams (or groups) that can be spatially multiplexed.

We define T_s as the number of scheduling windows, wherein mutually exclusive subsets of multicast groups are served, as shown in Fig 2. The admissible range of scheduling windows, T_s , depends on both N_{tx}^{RF} and G_T . Specifically,

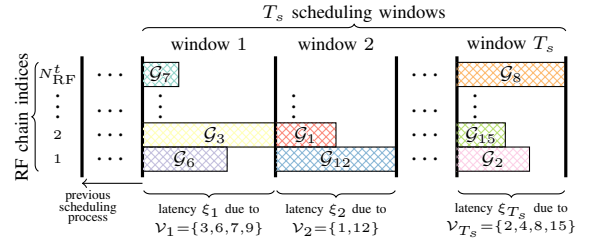


Figure 2: Multicast groups scheduling: Multicast groups 1 and 12 have been jointly scheduled during window $t = 2$.

$\lceil \frac{G_T}{N_{tx}^{RF}} \rceil \leq T_s \leq G_T$ is maximum when exactly one multicast group is served per scheduling window. Also, T_s is minimum when the gNodeB operates at maximal utilization, serving N_{tx}^{RF} multicast groups simultaneously during every window (except for at most one window, if $G_T \bmod N_{tx}^{RF} \neq 0$). Let \mathcal{V}_t denote an ordered set containing the indices of the co-scheduled groups within window t . In addition, \mathcal{U}_t denotes the set of receivers catered during window t , i.e. $\mathcal{U}_t = \{k \mid k \in \mathcal{G}_i, i \in \mathcal{V}_t\}$. Similarly, $\{\mathcal{V}_t\}_{t=1}^{T_s}$ and $\{\mathcal{U}_t\}_{t=1}^{T_s}$ denote the collection of \mathcal{V}_t and \mathcal{U}_t for all scheduling windows, respectively. Since every multicast group is served only once within T_s windows, then $\mathcal{V}_t \cap \mathcal{V}_{t'} = \{\emptyset\}, \mathcal{U}_t \cap \mathcal{U}_{t'} = \{\emptyset\}$. Due to the multicast nature of the system, every receiver $k \in \mathcal{G}_i$ requires the same length- B_i bit stream $\mathbf{b}_i = [b_{i1}, \dots, b_{iB_i}]^T$. Thus, the amount of bits required by receiver k is $B_k = B_i, \forall k \in \mathcal{G}_i$. At the transmitter, each bit stream \mathbf{b}_i is encoded at a suitable rate π_i that allows successful decoding at every intended receiver. As a result, G_T symbol streams $\tilde{\mathbf{s}}_i = [\tilde{s}_{i1}, \tilde{s}_{i2}, \dots]^T$ ($i \in \mathcal{I}$) with symbol-wise average unit power are produced, i.e., $\mathbb{E} \{\tilde{\mathbf{s}}_i \tilde{\mathbf{s}}_i^H\} = \mathbf{I}$. The symbol streams are arranged in a matrix $\mathbf{S} = [\tilde{\mathbf{s}}_1, \dots, \tilde{\mathbf{s}}_{G_T}]^T$ that is zero-padded where necessary, as the length of each stream $\tilde{\mathbf{s}}_i$ depends on B_i and π_i . Specifically, the non-zero entries of \mathbf{S} represent the effective data that needs to be delivered to all the groups (within T_s scheduling windows). Let $\hat{\mathbf{S}}_t = \mathbf{V}_t \mathbf{S}$ denote the $|\mathcal{V}_t|$ symbol streams transmitted during the t -th scheduling window, where $\mathbf{V}_t \in \{0, 1\}^{|\mathcal{V}_t| \times G_T}$ is a binary scheduling matrix that filters the symbol streams from \mathbf{S} . The *transmission latency* associated to the delivery of $\hat{\mathbf{S}}_t$ is defined as $\xi_t = \max_{i \in \mathcal{V}_t} \frac{B_i}{\pi_i}$, which represent the minimal time interval required by the devices in all the multicast groups $i \in \mathcal{V}_t$ to receive the intended data.

For any window t , the analog and digital precoders of the hybrid transmitter are denoted by $\mathbf{F}_t \in \mathbb{C}^{N_{tx} \times N_{tx}^{RF}}$ and $\mathbf{M}_t \in \mathbb{C}^{N_{tx}^{RF} \times |\mathcal{V}_t|}$, respectively. Any element (q, r) of the analog precoder is a phase rotation with constant modulus. Thus, $[\mathbf{F}_t]_{q,r} \in \mathcal{F}$, where $q \in \mathcal{Q} = \{(r-1)L_{tx} + l \mid 1 \leq l \leq L_{tx}\}, r \in \mathcal{R} = \{1, \dots, N_{tx}^{RF}\}$, and $\mathcal{F} = \left\{ \sqrt{\delta_F} \dots, \sqrt{\delta_F} e^{j \frac{2\pi(D_F-1)}{D_F}} \right\}$. D_F denotes the number of different phase shifts allowed at the transmitter, and δ_F is a scaling factor. The combiner of the k -th receiver is denoted by $\mathbf{w}_k \in \mathbb{C}^{N_{rx} \times 1}$, where $[\mathbf{w}_k]_l \in \mathcal{W}, l \in \mathcal{L} = \{1, \dots, N_{rx}\}$, $\mathcal{W} = \left\{ \sqrt{\delta_W} \dots, \sqrt{\delta_W} e^{j \frac{2\pi(D_W-1)}{D_W}} \right\}$, D_W is the number of phase shifts allowed at the analog combiner, and δ_W is a scaling factor. The instantaneous downlink signal is represented by $\mathbf{x}_t = \mathbf{F}_t \mathbf{M}_t \tilde{\mathbf{s}}$, where $\tilde{\mathbf{s}} = [\tilde{s}_{1c}, \dots, \tilde{s}_{|\mathcal{V}_t|c}]^T \in \mathbb{C}^{|\mathcal{V}_t| \times 1}$ sweeps through every column c of $\hat{\mathbf{S}}_t$ extracting the multicast symbols

to be delivered during window t . The received signal at the k -th device is denoted by $y_k = \mathbf{w}_k^H \mathbf{H}_k \mathbf{x}_t$, where $\mathbf{H}_k \in \mathbb{C}^{N_{rx} \times N_{tx}}$ denotes the channel between the device and the gNodeB, whereas $\mathbf{n}_k \sim \mathcal{CN}(0, \sigma^2 \mathbf{I})$ denotes additive white Gaussian noise. Assuming a flat-fading channel, y_k is given by

$$y_k = \underbrace{\mathbf{w}_k^H \mathbf{H}_k \mathbf{F}_t \mathbf{M}_t \mathbf{s}_{i_t}}_{\text{desired multicast signal}} + \underbrace{\mathbf{w}_k^H \mathbf{H}_k \sum_{j_t=1, j_t \neq i_t}^{|\mathcal{V}_t|} \mathbf{F}_t \mathbf{M}_t \mathbf{s}_{j_t}}_{\text{interference}} + \underbrace{\mathbf{w}_k^H \mathbf{n}_k}_{\text{noise}}, \quad (1)$$

where $i_t \in \{1, 2, \dots, |\mathcal{V}_t|\}$ is a relative index to denote the elements of \mathcal{V}_t . Also, $\mathbf{s}_{i_t} = \bar{\mathbf{s}} - \mathbf{s}_{j_t}$ is a vector that contains zeros except for the i_t -th position, which stores the i_t -th element of $\bar{\mathbf{s}}$. Thus, the SINR at receiver k is defined as

$$\text{SINR}_k = \frac{|\mathbf{w}_k^H \mathbf{H}_k \mathbf{F}_t \mathbf{M}_t \mathbf{e}_{i_t}|^2}{\sum_{j_t=1, j_t \neq i_t}^{|\mathcal{V}_t|} |\mathbf{w}_k^H \mathbf{H}_k \mathbf{F}_t \mathbf{M}_t \mathbf{e}_{j_t}|^2 + \sigma^2 \|\mathbf{w}_k\|_2^2}, \quad (2)$$

where \mathbf{e}_{i_t} stores a 1 in the i_t -th position if $k \in \mathcal{V}_t \{i_t\}$ or 0 otherwise. Based on [30], the achievable rate π is approximated by the modified Shannon capacity,

$$\pi = \min\{C, C_{\max}\}, \quad (3)$$

where $C = \log_2(1 + \beta \cdot \text{SINR})$, C_{\max} is the capacity limit and $\beta = 0.5$ represents the SINR loss [30]. In (1) and (2), we have dropped the subscript t when referring to \mathbf{w}_k because only the combiners of the scheduled receivers need to be designed.

Remark: \mathbf{V}_t is obtained from $\mathcal{V}_t = \{v_1^t, v_2^t, \dots\}$. For instance, if v_a^t ($a \in \{1, 2, \dots, |\mathcal{V}_t|\}$) is in the z -th position in \mathcal{V}_t , then the element in the z -th row and v_a^t -th column of \mathbf{V}_t is set to 1.

IV. SCHEDULING CRITERIA FOR MULTICASTING

Note that T_s is not necessarily related to the overall transmission latency $\xi = \sum_{t=1}^{T_s} \xi_t$. Each bit stream \mathbf{b}_i is to be transmitted at an optimal rate π_i that not only should provide service ubiquitousness (data decoding at every intended receiver) but also should minimize the transmission latency of the co-scheduled groups. Encoding every $\mathbf{b}_i \in \mathcal{V}_t$ at a high rate will promote low latency ξ_t , but it will require superior SINR at every receiver $k \in \mathcal{G}_i$ ($i \in \mathcal{V}_t$) to ensure successful decoding. Nevertheless, under constrained transmit and receive power, a high SINR at every receiver cannot be guaranteed, compromising thereby the service ubiquitousness. On the other hand, transmitting at very low rate improves data decodability for a larger number of receivers (ubiquitousness enhancement) at the expense of increasing latency. In light of this observation, we realize that the optimal rate needs to be carefully devised to (i) improve the ubiquitousness and (ii) minimize the latency. However, the optimal rate depends on the SINR, which can only be determined once the scheduling, precoder and combiners have been designed. This calls for a meticulous design of the hybrid precoder, analog combiners, and scheduling in order to attain ubiquitous multi-group multicast service with low latency. In the following, we present three propositions that will guide our design of $\{\mathcal{V}_t\}_{t=1}^{T_s}$, $\{\mathbf{F}_t\}_{t=1}^{T_s}$, $\{\mathbf{M}_t\}_{t=1}^{T_s}$, $\{\mathbf{w}_k\}_{k=1}^{K_T}$ to attain the desired objectives.

Proposition 1: Let $1 \leq t' \leq T_s$ be a window with defined $\mathcal{V}_{t'}$, $\mathbf{F}_{t'}$, $\mathbf{M}_{t'}$, $\{\mathbf{w}_k\}_{k \in \mathcal{U}_{t'}}$, then the transmission latency $\xi_{t'}|\mathcal{V}_{t'}, \mathbf{F}_{t'}, \mathbf{M}_{t'}, \{\mathbf{w}_k\}_{k \in \mathcal{U}_{t'}}$ is approximately inversely proportional

to the minimum regularized SINR (r -SINR) among all the co-scheduled receivers.

We assume that for a certain window t' , the sets $\mathcal{V}_{t'}$ and $\mathcal{U}_{t'}$ have been determined. Moreover, we consider that $\mathbf{F}_{t'}$ and $\mathbf{M}_{t'}$ at the transmitter, and $\{\mathbf{w}_k\}_{k \in \mathcal{U}_{t'}}$ for each scheduled receiver, have been designed. Under these assumptions, the SINR at any receiver is obtained via (2). The maximal rate $\pi_{k|\mathcal{V}_{t'}, \mathbf{F}_{t'}, \mathbf{M}_{t'}, \mathbf{w}_k}$ at which receiver $k \in \mathcal{G}_i$ ($i \in \mathcal{V}_{t'}$) can successfully decode is given by (3). Thus, the minimal latency associated to receiver $k \in \mathcal{G}_i$ ($i \in \mathcal{V}_{t'}$) is $\xi_{k|\mathcal{V}_{t'}, \mathbf{F}_{t'}, \mathbf{M}_{t'}, \mathbf{w}_k} = \frac{B_i}{\pi_{k|\mathcal{V}_{t'}, \mathbf{F}_{t'}, \mathbf{M}_{t'}, \mathbf{w}_k}}$. Since every receiver $k \in \mathcal{G}_i$ ($i \in \mathcal{V}_{t'}$) requires the same information, the optimal rate at which \mathbf{b}_i can be encoded while guaranteeing successful reception at every receiver, is determined by $\pi_{i|\mathcal{V}_{t'}, \mathbf{F}_{t'}, \mathbf{M}_{t'}, \{\mathbf{w}_k\}_{k \in \mathcal{U}_{t'}}} = \min_{k \in \mathcal{G}_i} \pi_{k|\mathcal{V}_{t'}, \mathbf{F}_{t'}, \mathbf{M}_{t'}, \mathbf{w}_k}$. The latency associated to multicast group $i \in \mathcal{V}_{t'}$ is denoted by $\xi_{i|\mathcal{V}_{t'}, \mathbf{F}_{t'}, \mathbf{M}_{t'}, \{\mathbf{w}_k\}_{k \in \mathcal{U}_{t'}}$, and the latency owing to all multicast groups scheduled during window t' is defined as $\xi_{t'}|\mathcal{V}_{t'}, \mathbf{F}_{t'}, \mathbf{M}_{t'}, \{\mathbf{w}_k\}_{k \in \mathcal{U}_{t'}} = \max_{i \in \mathcal{V}_{t'}} \xi_{i|\mathcal{V}_{t'}, \mathbf{F}_{t'}, \mathbf{M}_{t'}, \{\mathbf{w}_k\}_{k \in \mathcal{U}_{t'}}$, which can also be expressed as

$$\xi_{t'}^* = \xi_{t'}|\mathcal{U}_{t'}, \mathbf{F}_{t'}, \mathbf{M}_{t'}, \{\mathbf{w}_k\}_{k \in \mathcal{U}_{t'}} = \max_{k \in \mathcal{U}_{t'}} \left\{ \frac{B_k}{\pi_{k|\mathcal{U}_{t'}, \mathbf{F}_{t'}, \mathbf{M}_{t'}, \mathbf{w}_k}} \right\} \quad (4)$$

As shown in Appendix A, the transmission latency is approximately inversely proportional to the minimum r -SINR among all the receivers $k \in \mathcal{U}_{t'}$, i.e.,

$$\xi_{t'}^* \approx^{-1} \min_{k \in \mathcal{U}_{t'}} \left\{ \left(1 + \beta \cdot \text{SINR}_{k|\mathcal{V}_{t'}, \mathbf{F}_{t'}, \mathbf{M}_{t'}, \mathbf{w}_k}\right)^{\frac{1}{\beta}} \right\}, \quad (5)$$

where $(1 + \beta \cdot \text{SINR}_{k|\mathcal{V}_{t'}, \mathbf{F}_{t'}, \mathbf{M}_{t'}, \mathbf{w}_k})^{\frac{1}{\beta}}$ is termed r -SINR. Further, (5) reveals a crucial relation between latency and SINR, which we exploit to design optimal precoders and combiners.

Proposition 2: Let t' be a window with defined $\mathcal{V}_{t'}$, then the minimization of transmission latency $\xi_{t'}|\mathcal{V}_{t'}$ is equivalent to designing $\mathbf{F}_{t'}$, $\mathbf{M}_{t'}$, $\{\mathbf{w}_k\}_{k \in \mathcal{U}_{t'}}$ such that the minimum equalized SINR (e -SINR) of all co-scheduled receivers is maximized.

To minimize the latency associated to $\mathcal{V}_{t'}$, the optimization problem that devises optimal $\mathbf{F}_{t'}$, $\mathbf{M}_{t'}$, $\{\mathbf{w}_k\}_{k \in \mathcal{U}_{t'}}$ is

$$\min_{\substack{\mathbf{F}_{t'} \in \Omega_F \\ \mathbf{M}_{t'} \in \Omega_M \\ \{\mathbf{w}_k\}_{k \in \mathcal{U}_{t'}} \in \Omega_W}} \xi_{t'}|\mathcal{U}_{t'} \leftrightarrow \max_{\substack{\mathbf{F}_{t'} \in \Omega_F \\ \mathbf{M}_{t'} \in \Omega_M \\ \{\mathbf{w}_k\}_{k \in \mathcal{U}_{t'}} \in \Omega_W}} \min_{k \in \mathcal{U}_{t'}} \frac{\text{SINR}_{k|\mathcal{V}_{t'}}}{B_k}, \quad (6)$$

where $\frac{\text{SINR}_{k|\mathcal{V}_{t'}}}{B_k}$ is e -SINR. Also, Ω_F , Ω_M , and Ω_W are the feasible sets for the analog precoder, digital precoder and analog combiners, respectively. A more detailed derivation of this expression is available in Appendix B.

Proposition 3: The minimization of the overall transmission latency of the system is equivalent to simultaneously maximizing the minimum e -SINR of the co-scheduled receivers at every scheduling window.

It follows from Proposition 2 that, in order to minimize the overall latency, the latency associated to every scheduling window t must also be minimum. Thus,

$$\min_{\substack{\{\mathbf{F}_t\}_{t=1}^{T_s} \in \Omega_F \\ \{\mathbf{M}_t\}_{t=1}^{T_s} \in \Omega_M \\ \{\mathbf{w}_k\}_{k=1}^{K_T} \in \Omega_W \\ \{\mathcal{V}_t\}_{t=1}^{T_s} \in \Omega_V(T_s) \\ T_s \in \Omega_T}} \xi \leftrightarrow \max_{\substack{\{\mathbf{F}_t\}_{t=1}^{T_s} \in \Omega_F \\ \{\mathbf{M}_t\}_{t=1}^{T_s} \in \Omega_M \\ \{\mathbf{w}_k\}_{k=1}^{K_T} \in \Omega_W \\ \{\mathcal{V}_t\}_{t=1}^{T_s} \in \Omega_V(T_s) \\ T_s \in \Omega_T}} \bigwedge_{t=1}^{T_s} \min_{k \in \mathcal{U}_t} \left\{ \frac{\text{SINR}_{k|\mathcal{V}_t}}{B_k} \right\}, \quad (7)$$

where $\xi = [\xi_1, \dots, \xi_{T_s}]^T$. Besides, $\Omega_{V(T_s)}$ denotes the feasible set of all the scheduling combinations for a given T_s , whereas $\Omega_T \equiv [[G_T/N_{\text{tx}}^{\text{RF}}], G_T]$ defines the feasible set of T_s . Since the feasible sets Ω_F , Ω_M , Ω_W , $\Omega_{V(T_s)}$, and Ω_T are non-convex (discussed in Section V), (7) is difficult to solve. Moreover, $\{\mathbf{F}_t\}_{t=1}^{T_s}$, $\{\mathbf{M}_t\}_{t=1}^{T_s}$, and $\{\mathbf{w}_k\}_{k=1}^{K_T}$ are mutually coupled as observed in (2). Furthermore, the number of potential scheduling combinations grows combinatorially with G_T and $N_{\text{tx}}^{\text{RF}}$.

A straightforward but intractable solution to (7) is exhaustive search (XHAUS), whereby every scheduling pattern $\{\mathcal{V}_t\}_{t=1}^{T_s} \in \Omega_{V(T_s)}$ for every value $T_s \in \Omega_T$ is created. Then, for each pattern, the precoder and combiners are to be designed according to (6) while keeping the best-performing scheduling. A simpler approach consists in randomly associating the groups (RAND) and then solving (6). It is evident that for any scheduling choice, we are required to solve (6) for every window. Thus, in the following, we propose an approach based on semidefinite relaxation and Cholesky matrix factorization to design near-optimal hybrid precoders and analog combiners.

V. PROPOSED JOINT DESIGN OF HYBRID PRECODER AND ANALOG COMBINERS

Given \mathcal{V}_t , a suitable hybrid precoder and analog combiners for window t can be designed based on (6). Thus, the latency ξ_t is minimized when

$$\mathcal{P}_0 : \max_{\mathbf{F}_t, \mathbf{M}_t, \{\mathbf{w}_k\}_{k \in \mathcal{U}_t}} \min_{k \in \mathcal{U}_t} \frac{\frac{1}{B_k} |\mathbf{w}_k^H \mathbf{H}_k \mathbf{F}_t \mathbf{M}_t \mathbf{e}_{i_t}|^2}{\sum_{\substack{j_i=1 \\ j_i \neq i_t}} |\mathbf{w}_k^H \mathbf{H}_k \mathbf{F}_t \mathbf{M}_t \mathbf{e}_{j_t}|^2 + \sigma^2 \|\mathbf{w}_k\|_2^2} \quad (8a)$$

$$\text{s.t.} \quad \|\mathbf{F}_t \mathbf{M}_t\|_{\text{F}}^2 \leq P_{\text{tx}}^{\text{max}}, \quad (8b)$$

$$\|\mathbf{w}_k\|_2^2 \leq P_{\text{rx}}^{\text{max}}, k \in \mathcal{U}_t, \quad (8c)$$

$$[\mathbf{F}_t]_{q,r} \in \mathcal{F}, q \in \mathcal{Q}, r \in \mathcal{R}, \quad (8d)$$

$$[\mathbf{w}_k]_l \in \mathcal{W}, l \in \mathcal{L}, \quad (8e)$$

where (8a) aims at maximizing the minimum e-SINR, (8b) restricts the transmit power of the hybrid precoder, whereas (8c) limits the receive power of each receiver. On the other hand, (8d) and (8e) enforce the phase shifts of the analog precoder \mathbf{F}_t and analog combiners $\{\mathbf{w}_k\}_{k \in \mathcal{U}_t}$ to have constant modulus. Furthermore, (8a) is non-convex since it is as a fractional program of quadratic forms with coupled parameters. The constraints (8d) and (8e) are non-convex since $[\mathbf{F}_t]_{q,r}$ and $[\mathbf{w}_k]_l$ belong to the non-convex sets \mathcal{F} and \mathcal{W} , respectively. Thus, (8c) is also non-convex. Besides, (8b) is non-convex due to the coupling between \mathbf{F}_t and \mathbf{M}_t , and the existence of (8d). As a result, \mathcal{P}_0 is a non-convex program with non-convex constraints. Note that (8) can be recast as (9),

$$\mathcal{P}_0 : \max_{\substack{\alpha, \mathbf{F}, \mathbf{M}, \\ \{\mathbf{w}_k\}_{k=1}^K}} \alpha \quad (9a)$$

$$\text{s.t.} \quad \frac{1}{B_k} \frac{|\mathbf{w}_k^H \mathbf{H}_k \mathbf{F} \mathbf{M} \mathbf{e}_i|^2}{\sum_{j \neq i} |\mathbf{w}_k^H \mathbf{H}_k \mathbf{F} \mathbf{M} \mathbf{e}_j|^2 + \sigma^2 \|\mathbf{w}_k\|_2^2} \geq \alpha, \quad (9b)$$

$$\|\mathbf{F} \mathbf{M}\|_{\text{F}}^2 \leq P_{\text{tx}}^{\text{max}}, \quad (9c)$$

$$\|\mathbf{w}_k\|_2^2 \leq P_{\text{rx}}^{\text{max}}, \forall k \in \mathcal{U}_t, \quad (9d)$$

$$[\mathbf{F}]_{q,r} \in \mathcal{F}, q \in \mathcal{Q}, r \in \mathcal{R}, \quad (9e)$$

$$[\mathbf{w}_k]_l \in \mathcal{W}, l \in \mathcal{L}, \quad (9f)$$

$$\alpha \geq 0. \quad (9g)$$

For notation simplification, we assume that $G = |\mathcal{V}_t|$ and $K = |\mathcal{U}_t|$. In addition, we also drop the subscript t when referring to \mathbf{F}_t and \mathbf{M}_t . Note that \mathcal{P}_0 is challenging to solve due to parameter coupling and non-convexity of the feasible sets. In fact, for the particular case when $\mathbf{F} = \mathbf{I}$ and $\mathbf{w}_k = 1$, \mathcal{P}_0 was shown to be NP-hard [10]. In this paper, we resort to alternate optimization [31] to solve (9). Thus, \mathbf{F} , \mathbf{M} , and $\{\mathbf{w}_k\}_{k=1}^K$ are sequentially optimized in an iterative manner.

A. Optimization of \mathbf{F}

Given \mathbf{M} and $\{\mathbf{w}_k\}_{k=1}^K$, α and \mathbf{F} are optimized as follows,

$$\mathcal{P}_1 : \max_{\alpha, \mathbf{F}} \alpha \quad (10a)$$

$$\text{s.t.} \quad \alpha B_k \sum_{j \neq i} \left| \mathbf{w}_k^H \mathbf{H}_k \mathbf{F} \mathbf{M} \mathbf{e}_j \right|^2 + \alpha B_k \sigma^2 \|\mathbf{w}_k\|_2^2 - \left| \mathbf{w}_k^H \mathbf{H}_k \mathbf{F} \mathbf{M} \mathbf{e}_i \right|^2 \leq 0, \forall k \in \mathcal{U}_t, \quad (10b)$$

$$\|\mathbf{F} \mathbf{M}\|_{\text{F}}^2 \leq P_{\text{tx}}^{\text{max}}, \quad (10c)$$

$$[\mathbf{F}]_{q,r} \in \mathcal{F}, q \in \mathcal{Q}, r \in \mathcal{R}, \quad (10d)$$

$$\alpha \geq 0. \quad (10e)$$

Due to the sub-connected architecture of the analog precoder, \mathbf{F} is sparse. Thus, we can express $\mathbf{F} \mathbf{M} = \text{diag}(\mathbf{f}) \widetilde{\mathbf{M}}$, where $\widetilde{\mathbf{M}} = \mathbf{M} \otimes \mathbf{1}_{L_{\text{tx}}}$, and $\mathbf{f} \in \mathbb{C}^{N_{\text{tx}} \times 1}$ is a vector that contains the non-zero elements of \mathbf{F} . In addition, $\mathbf{F} \mathbf{M} \mathbf{e}_i = \text{diag}(\widetilde{\mathbf{M}} \mathbf{e}_i) \mathbf{f}$. Thus, (10) is equivalent to

$$\mathcal{P}_1 : \max_{\alpha, \mathbf{f}} \alpha \quad (11a)$$

$$\text{s.t.} \quad \alpha B_k \sum_{j \neq i} \mathbf{f}^H \mathbf{b}_{k,j} \mathbf{b}_{k,j}^H \mathbf{f} - \mathbf{f}^H \mathbf{b}_{k,i} \mathbf{b}_{k,i}^H \mathbf{f} + \alpha B_k \sigma^2 \|\mathbf{w}_k\|_2^2 \leq 0, \forall k \in \mathcal{U}_t, \quad (11b)$$

$$\|\mathbf{L} \mathbf{f}\|_2^2 \leq P_{\text{tx}}^{\text{max}}, \quad (11c)$$

$$[\mathbf{f}]_n \in \mathcal{F}, n \in \mathcal{N}, \quad (11d)$$

$$\alpha \geq 0, \quad (11e)$$

where $\mathbf{b}_{k,i} = \text{diag}(\widetilde{\mathbf{M}} \mathbf{e}_i)^H \mathbf{H}^H \mathbf{w}_k^H$, $\mathbf{L} = (\widetilde{\mathbf{M}}^T \otimes \mathbf{1}_{N_{\text{tx}}}) \odot (\mathbf{1}_G \otimes \mathbf{I}_{N_{\text{tx}} \times N_{\text{tx}}})$, $\mathcal{N} = \{1, 2, \dots, N_{\text{tx}}\}$. Realize that (11d) is non-convex due to the combinatorial selection of phase shifts $[\mathbf{f}]_n$ from \mathcal{F} . Similarly, (11b) and (11c) are non-convex as they depend on \mathbf{f} , whereas (11e) is linear. In order to approach \mathcal{P}_1 , our strategy consists of three stages. In the first stage (Stage A₁), we recast \mathcal{P}_1 as an SDR program to convexify (11b), (11c), and (11d), thus resulting in $\mathcal{P}_{\text{SDR},1}$ in (12). After convexification, the only non-convex constraint that remains in $\mathcal{P}_{\text{SDR},1}$ is (12b). To find a near-optimal solution, we resort to the bisection method in the second stage (Stage A₂). In the third stage (Stage A₃), we use Cholesky factorization and randomization to recover \mathbf{f} from \mathbf{Y} .

Stage A₁ (Transformation of \mathcal{P}_1 to SDR):

$$\mathcal{P}_{\text{SDR},1} : \max_{\alpha, \mathbf{Y}} \alpha \quad (12a)$$

$$\text{s.t.} \quad \alpha B_k \text{Tr}(\mathbf{B}_{k, \setminus i} \mathbf{Y}) - \text{Tr}(\mathbf{B}_{k,i} \mathbf{Y}) + \alpha B_k \sigma^2 \|\mathbf{w}_k\|_2^2 \leq 0, \forall k \in \mathcal{U}_t, \quad (12b)$$

$$\text{Tr}(\mathbf{D}\mathbf{Y}) \leq P_{\text{tx}}^{\max}, \quad (12c)$$

$$\text{diag}(\mathbf{Y}) = \delta_F \mathbf{1}_{N_{\text{tx}}}, \quad (12d)$$

$$\mathbf{Y} \succcurlyeq 0, \quad (12e)$$

$$\alpha \geq 0, \quad (12f)$$

where $\mathbf{Y} = \mathbf{f}\mathbf{f}^H$, $\mathbf{D} = \mathbf{L}^H\mathbf{L}$, $\mathbf{B}_{k,\setminus i} = \sum_{j \neq i} \mathbf{b}_{k,j} \mathbf{b}_{k,j}^H$ and $\mathbf{B}_{k,i} = \mathbf{b}_{k,i} \mathbf{b}_{k,i}^H$ are positive semi-definite matrices.

Stage A₂ (*Bisection search for $\mathcal{P}_{\text{SDR},1}$*): Notice that (12b) is quasi-convex on \mathbf{Y} and α because for any $\alpha \geq 0$, (12b) collapses to a convex constraint. Thus, we resort to the bisection search method [10], [22], [32], where we define an initial interval $[\alpha_L^{(0)}, \alpha_U^{(0)}]$ for α . Then, we progressively update the interval depending on the returned solutions for \mathbf{Y} . A natural lower bound is $\alpha_L^{(0)} = 0$. An upper bound $\alpha_U^{(0)}$ can be obtained by assigning the total power to the weakest receiver $k \in \mathcal{U}_t$. Thus, from (12b) we obtain $\alpha_U^{(0)} = \min_{k \in \mathcal{U}_t} \frac{\text{Tr}(\mathbf{B}_{k,i} \mathbf{Y})}{B_k \sigma^2 \|\mathbf{w}_k\|_2^2}$. Further, since $\mathbf{B}_{k,i}$ and \mathbf{Y} are positive semidefinite, $\text{Tr}(\mathbf{B}_{k,i} \mathbf{Y}) \leq \text{Tr}(\mathbf{B}_{k,i}) \text{Tr}(\mathbf{Y})$ holds [33]. Also, $\text{Tr}(\mathbf{Y}) = \text{Tr}(\mathbf{f}\mathbf{f}^H) = N_{\text{tx}}^{\text{RF}}$. Therefore, $\alpha_U^{(0)} = \min_{k \in \mathcal{U}_t} \frac{N_{\text{tx}}^{\text{RF}} \text{Tr}(\mathbf{B}_{k,i})}{B_k \sigma^2 \|\mathbf{w}_k\|_2^2}$. With the initial interval

defined, at every iteration ℓ we set $\alpha^{(\ell)} = \frac{\alpha_L^{(\ell)} + \alpha_U^{(\ell)}}{2}$ and solve $\mathcal{P}_{\text{SDR},1}^{(\ell)}$ for \mathbf{Y} with the given $\alpha^{(\ell)}$. At each iteration ℓ , we update the lower and upper bounds in the following manner. If $\mathcal{P}_{\text{SDR},1}^{(\ell)}$ is feasible, then $\alpha_L^{(\ell+1)} = \alpha^{(\ell)}$. Otherwise, $\alpha_U^{(\ell+1)} = \alpha^{(\ell)}$. Through this procedure, an ϵ -suboptimal solution can be obtained within $N_{\text{bis}_1} = \log_2 \left(\frac{1}{\epsilon} (\alpha_U^{(0)} - \alpha_L^{(0)}) \right)$ iterations.

Stage A₃ (*Recovery of \mathbf{f}*): Let $\hat{\mathbf{Y}}$ represent an ϵ -suboptimal solution to (12). When $\hat{\mathbf{Y}}$ is rank-1, an optimal solution $\mathbf{Y}^* = \hat{\mathbf{Y}}$ has been found to (12). Thus, \mathbf{f}^* can be recovered straightforwardly by means of eigen-decomposition. Otherwise, we resort to a procedure inspired by [34].

Stage A_{3.1}: Any element (n_1, n_2) of \mathbf{Y} can be represented as $[\mathbf{Y}]_{n_1, n_2} = [\mathbf{f}]_{n_1} [\mathbf{f}]_{n_2}^*$. If we define a vector $\mathbf{u} \in \mathbb{C}^{N_{\text{tx}} \times 1}$ such that $\|\mathbf{u}\|_2^2 = \mathbf{u}^H \mathbf{u} = 1$, we can express $[\mathbf{Y}]_{n_1, n_2}$ in terms of \mathbf{u} , i.e., $[\mathbf{Y}]_{n_1, n_2} = ([\mathbf{f}]_{n_1} \mathbf{u}^T) ([\mathbf{f}]_{n_2}^* \mathbf{u}^*)$. Moreover, if we define $\mathbf{q}_n = [\mathbf{f}]_n \mathbf{u}$, \mathbf{Y} can be recast as $\mathbf{Y} = \mathbf{Q}^T \mathbf{Q}^*$ with $\mathbf{Q} = [\mathbf{q}_1, \dots, \mathbf{q}_{N_{\text{tx}}}]$.

Stage A_{3.2}: By means of Cholesky factorization, we can decompose $\hat{\mathbf{Y}}$ as $\hat{\mathbf{Y}} = \hat{\mathbf{Q}}^T \hat{\mathbf{Q}}^*$, where $\hat{\mathbf{Q}} = [\hat{\mathbf{q}}_1, \dots, \hat{\mathbf{q}}_{N_{\text{tx}}}]$. In *Stage A_{3.1}*, we assumed that every \mathbf{q}_n is originated from the same vector \mathbf{u} . Thus, we need to find both \mathbf{f} and \mathbf{u} that satisfy $\mathbf{q}_n = [\mathbf{f}]_n \mathbf{u}$, $\forall n \in \mathcal{N}$. Since such vectors \mathbf{f} and \mathbf{u} may not exist, we aim at finding approximate $\hat{\mathbf{u}}$ and $\hat{\mathbf{f}}$, such that $\hat{\mathbf{q}}_n \approx [\hat{\mathbf{f}}]_n \hat{\mathbf{u}}$, $\forall n \in \mathcal{N}$. Mathematically, this is expressed as

$$\hat{\mathcal{P}}_{\text{LS},1} : \min_{\hat{\mathbf{u}}, \hat{\mathbf{f}}} \sum_{n=1}^{N_{\text{tx}}} \|\hat{\mathbf{q}}_n - [\hat{\mathbf{f}}]_n \hat{\mathbf{u}}\|_2^2 \quad (13a)$$

$$\text{s.t.} \quad \|\hat{\mathbf{u}}\|_2^2 = 1, \quad (13b)$$

$$[\hat{\mathbf{f}}]_n \in \mathcal{F}, \forall n \in \mathcal{N}, \quad (13c)$$

where we find $\hat{\mathbf{u}}$ and $\hat{\mathbf{f}}$ with the least error in the 2-norm sense.

Stage A_{3.3}: Minimizing simultaneously both $\hat{\mathbf{u}}$ and $\hat{\mathbf{f}}$ is challenging. Thus, we generate a random vector $\hat{\mathbf{u}}$, such that $\|\hat{\mathbf{u}}\|_2^2 = 1$. Therefore, we solve

$$\hat{\mathcal{P}}_{\text{LS},2} : \min_{[\hat{\mathbf{f}}]_n \in \mathcal{F}, \forall n \in \mathcal{N}} \sum_{n=1}^{N_{\text{tx}}} \|\hat{\mathbf{q}}_n - [\hat{\mathbf{f}}]_n \hat{\mathbf{u}}\|_2^2 \quad (14)$$

By expanding (14), we obtain

$$\hat{\mathcal{P}}_{\text{LS},2} : \max_{[\hat{\mathbf{f}}]_n \in \mathcal{F}, \forall n \in \mathcal{N}} \sum_{n=1}^{N_{\text{tx}}} \Re \left([\hat{\mathbf{f}}]_n \hat{\mathbf{q}}_n^H \hat{\mathbf{u}} \right). \quad (15)$$

Note that (15) can be decomposed into N_{tx} parallel sub-problems. Further, since $z_n = \hat{\mathbf{q}}_n^H \hat{\mathbf{u}}$ is known in $\hat{\mathcal{P}}_{\text{LS},2}$, we select $[\hat{\mathbf{f}}]_n$ such that the real part is maximized. This is equivalent to choosing $[\hat{\mathbf{f}}]_n$ with the closest phase to z_n^* . Therefore, among the phase rotations in \mathcal{F} , we choose the closest to z_n^* . To improve $\hat{\mathbf{f}}$, we generate N_{rand_1} vectors $\hat{\mathbf{u}}_v$ with $\|\hat{\mathbf{u}}_v\|_2^2 = 1$ ($v = 1, \dots, N_{\text{rand}_1}$), and for each we find its corresponding $\hat{\mathbf{f}}_v$. Then, we select $\hat{\mathbf{f}}^\dagger$ among N_{rand_1} candidates that provides the largest minimum e-SINR, i.e., $\hat{\mathbf{f}}^\dagger = \arg \max_{\hat{\mathbf{f}}_1, \dots, \hat{\mathbf{f}}_{N_{\text{rand}_1}}} \min_{k \in \mathcal{U}_t} \frac{\text{SINR}_k}{B_k}$. Finally, $\hat{\mathbf{f}}^\dagger$ is reshaped to obtain $\mathbf{F}^\dagger = \text{reshape}(\hat{\mathbf{f}}^\dagger)$. The function $\text{reshape}(\cdot)$ reverses the effect of $\text{vec}(\cdot)$.

B. Optimization of M

Assuming that \mathbf{F} and $\{\mathbf{w}_k\}_{k=1}^K$ are known, (9) collapses to

$$\mathcal{P}_2 : \max_{\alpha, \mathbf{M}} \alpha \quad (16a)$$

$$\text{s.t.} \quad \alpha B_k \sum_{j \neq i} \left| \mathbf{w}_k^H \mathbf{H}_k \mathbf{F} \mathbf{M} \mathbf{e}_j \right|^2 + \alpha B_k \sigma^2 \|\mathbf{w}_k\|_2^2 - \left| \mathbf{w}_k^H \mathbf{H}_k \mathbf{F} \mathbf{M} \mathbf{e}_i \right|^2 \leq 0, \forall k \in \mathcal{U}_t, \quad (16b)$$

$$\|\mathbf{F} \mathbf{M}\|_{\text{F}}^2 \leq P_{\text{tx}}^{\max}, \quad (16c)$$

$$\alpha \geq 0. \quad (16d)$$

We can equivalently express \mathcal{P}_2 as,

$$\mathcal{P}_2 : \max_{\alpha, \mathbf{m}} \alpha \quad (17a)$$

$$\text{s.t.} \quad \alpha B_k \sum_{j \neq i} \mathbf{m}^H \mathbf{c}_{k,j} \mathbf{c}_{k,j}^H \mathbf{m} - \mathbf{m}^H \mathbf{c}_{k,i} \mathbf{c}_{k,i}^H \mathbf{m} + \alpha B_k \sigma^2 \|\mathbf{w}_k\|_2^2 \leq 0, \forall k \in \mathcal{U}_t, \quad (17c)$$

$$\|(\mathbf{I} \otimes \mathbf{F}) \mathbf{m}\|_2^2 \leq P_{\text{tx}}^{\max}, \quad (17d)$$

$$\alpha \geq 0, \quad (17e)$$

where $\mathbf{c}_{k,i} = (\mathbf{e}_i \otimes (\mathbf{F}^H \mathbf{H}_k^H \mathbf{w}_k))$ and $\mathbf{m} = \text{vec}(\mathbf{M})$. Following a similar procedure as before, the SDR form of (17) is

$$\mathcal{P}_{\text{SDR},2} : \max_{\alpha, \mathbf{Z}} \alpha \quad (18a)$$

$$\text{s.t.} \quad \alpha B_k \text{Tr}(\mathbf{C}_{k,\setminus i} \mathbf{Z}) - \text{Tr}(\mathbf{C}_{k,i} \mathbf{Z}) + \alpha B_k \sigma^2 \|\mathbf{w}_k\|_2^2 \leq 0, \forall k \in \mathcal{U}_t, \quad (18b)$$

$$\text{Tr}(\mathbf{J} \mathbf{Z}) \leq P_{\text{tx}}^{\max}, \quad (18c)$$

$$\mathbf{Z} \succcurlyeq 0, \quad (18d)$$

$$\alpha \geq 0, \quad (18e)$$

where $\mathbf{Z} = \mathbf{m} \mathbf{m}^H$, $\mathbf{J} = (\mathbf{I} \otimes \mathbf{F})^H (\mathbf{I} \otimes \mathbf{F})$, $\mathbf{C}_{k,\setminus i} = \sum_{j \neq i} \mathbf{c}_{k,j} \mathbf{c}_{k,j}^H$ and $\mathbf{C}_{k,i} = \mathbf{c}_{k,i} \mathbf{c}_{k,i}^H$. As in Stage A₂, we use the bisection method to approach (18). In this case, $\alpha_L^{(0)} = 0$ and $\alpha_U^{(0)} = \min_{k \in \mathcal{U}_t} \frac{P_{\text{tx}}^{\max} \text{Tr}(\mathbf{C}_{k,i})}{B_k \sigma^2 \|\mathbf{w}_k\|_2^2}$. The process is repeated for N_{bis_2} iterations. At the end of the bisection procedure, we obtain $\hat{\mathbf{Z}}$ from which $\hat{\mathbf{m}}$ is estimated. If $\hat{\mathbf{Z}}$ is rank-1, then an optimal solution $\mathbf{Z}^* = \hat{\mathbf{Z}}$ has been found to (18). Otherwise, we generate N_{rand_2} candidates according to $\hat{\mathbf{m}}_v \sim \mathcal{CN}(\mathbf{0}, \hat{\mathbf{Z}})$ ($v = 1, \dots, N_{\text{rand}_2}$) and retain the best-performing candidate $\hat{\mathbf{m}}^\dagger = \arg \max_{\hat{\mathbf{m}}_1, \dots, \hat{\mathbf{m}}_{N_{\text{rand}_2}}} \min_{k \in \mathcal{U}_t} \frac{\text{SINR}_k}{B_k}$ [35], [36]. Finally, $\hat{\mathbf{m}}^\dagger$ is reshaped to obtain \mathbf{M}^\dagger .

C. Optimization of $\{\mathbf{w}_k\}_{k=1}^K$

Now, we assume that \mathbf{F} and \mathbf{M} are given. Therefore, we optimize the analog combiners $\{\mathbf{w}_k\}_{k=1}^K$ as shown in (19)

$$\mathcal{P}_3 : \max_{\alpha, \{\mathbf{w}_k\}_{k=1}^K} \alpha \quad (19a)$$

$$\text{s.t.} \quad \alpha B_k \sum_{j \neq i} \left| \mathbf{w}_k^H \mathbf{H}_k \mathbf{F} \mathbf{M} \mathbf{e}_j \right|^2 + \alpha B_k \sigma^2 \|\mathbf{w}_k\|_2^2 - \left| \mathbf{w}_k^H \mathbf{H}_k \mathbf{F} \mathbf{M} \mathbf{e}_i \right|^2 \leq 0, \forall k \in \mathcal{U}_t, \quad (19b)$$

$$\|\mathbf{w}_k\|_2^2 \leq P_{\text{rx}}^{\max}, \forall k \in \mathcal{U}_t, \quad (19c)$$

$$[\mathbf{w}_k]_l \in \mathcal{W}, l \in \mathcal{L}, \quad (19d)$$

$$\alpha \geq 0. \quad (19e)$$

We observe that each combiner can be optimized independently since any variation of \mathbf{w}_k will only affect the SINR of the k -th receiver. Therefore, we solve K sub-problems $\mathcal{P}_3^{(k)}$ in parallel. The SDR form of $\mathcal{P}_3^{(k)}$ is

$$\mathcal{P}_{\text{SDR},3}^{(k)} : \max_{\alpha, \mathbf{W}_k} \alpha \quad (20a)$$

$$\text{s.t.} \quad \alpha B_k \text{Tr}(\tilde{\mathbf{P}}_{k,\setminus i} \mathbf{W}_k) - \text{Tr}(\mathbf{P}_{k,i} \mathbf{W}_k), \quad (20b)$$

$$\text{Tr}(\mathbf{W}_k) \leq P_{\text{rx}}^{\max}, \quad (20c)$$

$$\text{diag}(\mathbf{W}_k) = \delta_W \mathbf{1}_{N_{\text{rx}}}, \quad (20d)$$

$$\mathbf{W}_k \succeq 0, \quad (20e)$$

$$\alpha \geq 0, \quad (20f)$$

where $\mathbf{W}_k = \mathbf{w}_k \mathbf{w}_k^H$, $\mathbf{P}_{k,i} = \mathbf{H}_k \mathbf{F} \mathbf{M} \mathbf{e}_i \mathbf{e}_i^H \mathbf{M}^H \mathbf{F}^H \mathbf{H}_k$ and $\tilde{\mathbf{P}}_{k,\setminus i} = \sum_{j \neq i} \mathbf{P}_{k,j} + B_k \sigma^2 \mathbf{I}$. Since the combiners \mathbf{w}_k are analog, we follow the same procedure used to optimize \mathbf{F} . In this case, the lower bound is $\alpha_{L_k}^{(0)} = 0$ whereas the upper bound $\alpha_{U_k}^{(0)} = \lambda_{\max}(\mathbf{P}_{k,i} \tilde{\mathbf{P}}_{k,\setminus i}^{-1})$ is the maximum eigenvalue of matrix $\mathbf{P}_{k,i} \tilde{\mathbf{P}}_{k,\setminus i}^{-1}$. The bisection process is repeated for N_{bis_3} iterations as explained in Stage A₂, upon whose completion $\widehat{\mathbf{W}}_k$ is obtained. If $\widehat{\mathbf{W}}_k$ is rank-1, then $\mathbf{W}_k^* = \widehat{\mathbf{W}}_k$ is also optimal to (20). Otherwise we generate N_{rand_3} candidates $\widehat{\mathbf{w}}_{k,v}$ ($v = 1, \dots, N_{\text{rand}_3}$) for each $\widehat{\mathbf{w}}_k$ as discussed in Stage A₃, and select the best-performing $\mathbf{w}_k^* = \arg \max_{\widehat{\mathbf{w}}_{k,1}, \dots, \widehat{\mathbf{w}}_{k,N_{\text{rand}_3}}} \frac{\text{SINR}_k}{B_k}$.

To further refine \mathbf{F} , \mathbf{M} , $\{\mathbf{w}_k\}_{k=1}^K$, we sequentially solve $\mathcal{P}_{\text{SDR},1}$, $\mathcal{P}_{\text{SDR},2}$ and $\{\mathcal{P}_{\text{SDR},3}^{(k)}\}_{k=1}^K$ for a number of N_{iter} iterations. Also, since the number of bits B_i to be transmitted can be arbitrarily large, we use normalized values \tilde{B}_i in the range $[0, 1]$, only for optimization purposes. Also, the scaling factors δ_F and δ_W , in Section III, are chosen such that $\|\mathbf{F}\|_{\text{F}}^2 = N_{\text{tx}}^{\text{RF}}$ and $\|\mathbf{w}_k\|_2^2 = P_{\text{rx}}^{\max}$. Thus, $\delta_F = N_{\text{tx}}^{\text{RF}}/N_{\text{tx}}$ and $\delta_W = P_{\text{rx}}^{\max}/N_{\text{rx}}$.

VI. PROPOSED SCHEDULING ALGORITHM

Given that scheduling plays a key role in ensuring minimum latency, in this section, we propose a novel scheduling formulation that aims to minimize both, the number of scheduling windows and the aggregate inter-group correlation (IGC). We model the scheduling problem as a Boolean program,

$$\mathcal{S} : \min_{\{\mu_{i,i}\}_{i=1}^{G_T}, \{\tau_{i,j,l}\}} \underbrace{\sum_{i=1}^{G_T} \mu_{i,i}}_{\text{first term}} + \omega \underbrace{\sum_{i=1}^{G_T-1} \sum_{j \geq i} \sum_{l > j} \rho_{j,l} \cdot \tau_{i,j,l}}_{\text{second term: aggregate IGC}} \quad (21a)$$

$$\text{s.t.} \quad \sum_{i \leq j < l} \rho_{j,l} \cdot \tau_{i,j,l} \leq \lambda \cdot \mu_{i,i}, \forall i, \quad (21b)$$

$$\sum_{i \leq j} \mu_{i,j} = 1, \forall j, \quad (21c)$$

$$\sum_{j \geq i} \mu_{i,j} \leq N_{\text{tx}}^{\text{RF}}, \forall i, \quad (21d)$$

$$\mu_{i,j} \leq \mu_{i,i}, \forall i < j, \quad (21e)$$

$$\mu_{i,j} + \mu_{i,l} \leq 1 + \tau_{i,j,l}, \forall i \leq j < l, \quad (21f)$$

$$\mu_{i,j} \in \{0, 1\}, \quad (21g)$$

$$\tau_{i,j,l} \in \{0, 1\}. \quad (21h)$$

Each binary variable $\mu_{i,j}$ assumes the value of 1 if multicast group j is scheduled in the i -th window (or 0 otherwise). The binary variable $\tau_{i,j,l}$ is 1 if any two multicast groups j and l have been co-scheduled during the i -th window. Also, we define $\rho_{j,l} = \frac{|\mathbf{h}_j^H \mathbf{h}_l|}{\|\mathbf{h}_j\|_2 \|\mathbf{h}_l\|_2}$ as the inter-group correlation (IGC) between groups j and l , where $\mathbf{h}_j = \frac{1}{|\mathcal{G}_j|} \sum_{k \in \mathcal{G}_j} \text{vec}(\mathbf{H}_k)$ is the mean channel vector of all receivers k in group j . The first term in (21a) represents the number of scheduling windows, whereas the second term is the aggregate IGC, which is computed in a pair-wise manner and accumulated as a penalization. If there exist more than a solution that yields the same optimal amount of scheduling windows, the second term penalizes the candidates that exhibit large aggregate IGC. Realize that by minimizing the aggregate IGC, we attempt to produce scheduling patterns wherein receivers of different co-scheduled groups are the least correlated (on average), thereby enhancing the SINR and latency. For every window i , (21b) restricts the aggregate IGC of the co-scheduled groups to remain below λ , which is the maximum threshold. Also, (21c) enforces every group j to be scheduled once, whereas (21d) restricts the number of groups per window to be at most $N_{\text{tx}}^{\text{RF}}$. Without loss of generality, (21e) and the condition $i < j$ imposed on (21a)–(21d) reduce the search space and therefore the complexity. Further, (21f) binds the variables $\mu_{i,j}$ and $\tau_{i,j,l}$ and ensures consistency among them. Finally, (21g) and (21h) declare $\mu_{i,i}$ and $\tau_{i,j,l}$ as Boolean. In (21a), ω is chosen such that the first and second term have equal weights on average.

VII. NUMERICAL RESULTS

This section sheds light on the performance of our proposed scheme **HYDRAWAVE** (joint group scheduling and precoding). We focus on two performance metrics: *minimum e-SINR* and *latency*. First, to gain insights into the effectiveness of our hybrid precoder design, we evaluate its performance against fully-digital and fully-analog implementations, in which we leave out the scheduling aspect. Next, we investigate the impact of different scheduling algorithms on the total latency, which additionally accounts for the beam-switching delay between the scheduling windows.

HYDRAWAVE: our proposed scheduling and precoding scheme.
SING: single-group multicasting scheduling serves only one multicast group per scheduling window.

RAND: random scheduling selects stochastically an allocation pattern among all possible combinations.

XHAUS: exhaustive search finds the best scheduling policy that minimizes latency among all the possibilities.

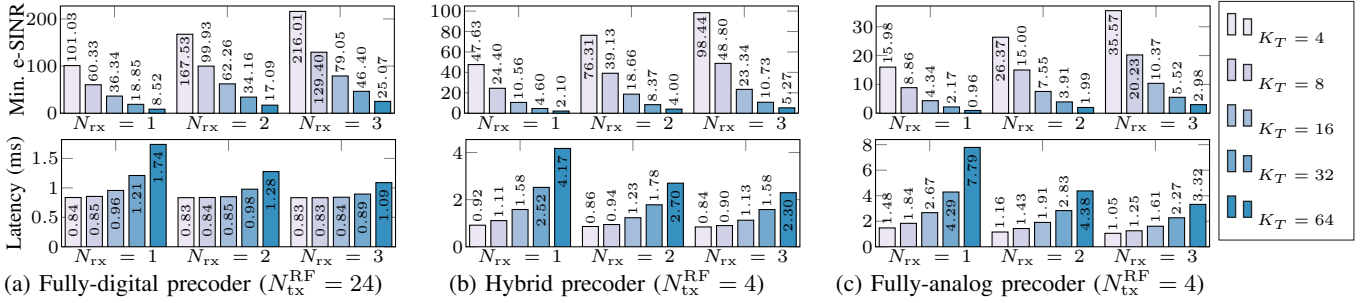


Figure 3: Evaluation of e-SINR and latency for different precoders

In simulations, we consider the geometric channel model with $N_{\text{paths}} = 6$ propagation paths between the transmitter and each receiver [37], [38], considering the high density of reflecting surfaces in an industrial environment. The receivers are divided equally among all the multicast groups. The numerical results show the average performance over 100 channel realizations. Table II summarizes the parameters setting.

Table II: Simulations configuration

Parameter	Notation & Value
Number of antennas at the transmitter	$N_{\text{tx}} = 24$ (with $L_{\text{tx}} = 6$)
Number of antennas at the receiver	$N_{\text{rx}} = \{1, 2, 3\}$
Number of RF chains at the transmitter	$N_{\text{tx}}^{\text{RF}} = 4$
Number of shifts at the transmitter	$D_F = 16$
Number of phase shifts at the receivers	$D_W = 4$
Maximum transmit power	$P_{\text{tx}}^{\text{max}} = 20$ dBm (100 mW)
Maximum receive power	$P_{\text{rx}}^{\text{max}} = 0$ dBm (1 mW)
Noise power	$\sigma^2 = 10$ dBm
Number of multicast groups	$G_T = 4$
Number of receivers	$K_T = \{4, 8, 16, 32, 64\}$
Bit-stream length	$B_1 = B_2 = B_3 = B_4 = 4$ Mbits
Number of bisection procedures	$N_{\text{bis}_1} = N_{\text{bis}_2} = N_{\text{bis}_3} = 10$
Number of randomizations	$N_{\text{rand}_1} = 5 \cdot N_{\text{tx}}$
	$N_{\text{rand}_2} = 100 \cdot G_T $
	$N_{\text{rand}_3} = 20 \cdot N_{\text{rx}}$
Number of sequential iterations	$N_{\text{iter}} = 3$

1) Performance of Hybrid Precoder without Scheduling:

We compare the performance of the proposed hybrid precoder design against a fully-digital implementation, which can be obtained as a particular case of our formulation when $N_{\text{tx}}^{\text{RF}} = N_{\text{tx}}$, $L_{\text{tx}} = 1$ and $\mathbf{F} = \mathbf{I}$. Similarly, we also consider a fully-analog precoder that can be obtained when $\mathbf{M} = \mathbf{I}$. In this scenario, we consider a single window t' with a defined scheduling $\mathcal{V}_{t'}$, where two multicast groups are concurrently served. The performance of this scenario is shown in Fig. 3 and is essentially related to *Proposition 2*. We observe that, for a given number of receivers K_T , the minimum e-SINR improves with an increasing number of receive antennas N_{rx} , because the beam-steering capability of each receiver is augmented. Further, for a given N_{rx} , as the number of receivers K_T increases, the e-SINR reduces since the total power is distributed accordingly. In terms of latency, (calculated with (4)), the fully-digital precoder outperforms the hybrid and fully-analog precoders as it is endowed with a larger amount of RF chains that allows enhanced interference reduction, thus promoting higher data rates. However, due to excessive power consumption and hardware costs of fully-digital precoders in mmWave frequencies, the hybrid precoder is a promising candidate with low power consumption and high performance. For instance, if $P_{\text{RF}} = 250$ mW [39] and

$P_{\text{PS}} = 30$ mW [40] represent the power consumed by a single RF chain and a single 4-bit-resolution phase shifter ($D_F = 16$), the instantaneous power consumed by the hybrid and digital precoders are $P_{\text{hyb}} = P_{\text{tx}}^{\text{max}} + N_{\text{tx}}^{\text{RF}} P_{\text{RF}} + N_{\text{tx}} P_{\text{PS}} = 1.82$ W and $P_{\text{dig}} = P_{\text{tx}}^{\text{max}} + N_{\text{tx}}^{\text{RF}} P_{\text{RF}} = 6.10$ W, respectively. This reveals an improvement of 235% on energy consumption and 44%–232% on energy efficiency (results excluded due to space limitation).

2) Performance of Hybrid Precoder with Scheduling:

Fig. 4 illustrates the performance of HYDRAWAVE against SING, RAND, and XHAUS. In our scheduling formulation in (21), λ controls the maximum tolerable aggregate IGC. Thus, in the fully-digital precoder case, a larger λ can be supported due to the versatility of the precoder to manage interference. On the other hand, due to the limited amount of RF chains, the values of λ used with the hybrid and analog precoders need to be comparatively smaller. We observe that, in terms of latency, the fully-digital precoder outperforms the hybrid and fully-analog implementations. Further, for any precoder type with a small number of receivers (e.g., $K_T = 16$), SING produces the greatest latency while XHAUS is optimal (according to *Proposition 3*). On the other hand, RAND exhibits an intermediate performance between SING and XHAUS. As the number of receivers increases (e.g., $K_T = 64$), the performance gap between SING and XHAUS reduces considerably because interference becomes more complex to manage, thus yielding SING optimal in some realizations. On the contrary, RAND deteriorates since the impact of scheduling becomes more relevant in the presence of higher interference. When considering a switching delay of $\delta_{\text{SW}} = 0.5$ ms between consecutive windows [7], similar behavior can be observed except for SING being heavily penalized due to the incapability of spatial multiplexing. Furthermore, we include the performance of HYDRAWAVE with different values of λ . In Fig. 4, λ_{opt} is obtained upon evaluating several λ and bisecting the search space until negligible variation is observed. For the fully-digital precoder, HYDRAWAVE attains near-optimality when $K_T = 16$. Also, its performance remains within 11% of the optimal value for $K_T = \{32, 64\}$ when $\delta_{\text{SW}} = 0.0$, and within 9% when $\delta_{\text{SW}} = 0.5$ ms. In the hybrid and fully-analog cases, the performance of HYDRAWAVE remains in the range 1.5–9.5% and 3.4–11.7% of the optimal XHAUS, respectively. In the hybrid precoder case, HYDRAWAVE exhibits gains up 32% higher than SING and up to 102% compared to RAND when $\delta_{\text{SW}} = 0$. When $\delta_{\text{SW}} = 0.5$, the gains are up to 60% and 59%, respectively. While finding λ_{opt} could be time-consuming, we notice that

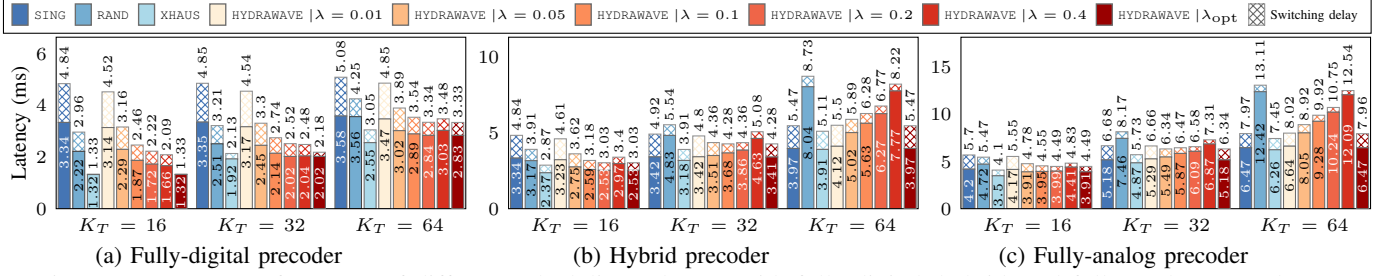


Figure 4: Latency performance of different scheduling schemes with fully-digital, hybrid, and fully-analog precoders.

for a reasonable value of $\lambda = \{0.05, 0.1\}$ the fully-digital and hybrid precoders behave suitably as compared to XHAUS while outperforming SING and RAND.

VIII. DISCUSSION AND FUTURE WORK

Optimization Parameters: Finding λ_{opt} could be challenging as it depends on the channel between the transmitter and receivers, as well as on the total interference which is related to the number of RF chains. In order to circumvent this problem, a system could be trained using deep-learning to map the inputs to a suitable value of λ . Other options to explore are data clustering and multivariate regression.

Hybrid Precoder Design: Compared to most approaches on hybrid precoding (multi-user or multicast) in the literature, in this paper, the hybrid precoder is not obtained as an approximation of the optimal digital implementation. We design the precoder without any knowledge of the digital implementation. We presume that the performance of the hybrid precoder can be further boosted if a better initialization scheme is explored.

Hybrid Precoder Complexity: Following the notation in (9), the worst-case complexity of the hybrid precoder design, when using standard interior-point methods is $N_{\text{bis}_1} \mathcal{O}(G^3 N_{\text{tx}}^6 + KGN_{\text{tx}}^2) + N_{\text{bis}_2} \mathcal{O}((GN_{\text{tx}}^{\text{RF}})^6 + K(GN_{\text{tx}}^{\text{RF}})^2) + KN_{\text{bis}_3} \mathcal{O}(N_{\text{tx}}^6 + N_{\text{rx}}^2)$.

Optimal Scheduler: Finding the optimal scheduler is intrinsically of combinatorial nature. Alternative relaxations of 0–1 parameters in *Proposition 3* based on \log , \exp , and \arctan functions could be further explored.

IX. CONCLUSION

We investigated the joint optimization of scheduling and multi-group multicast hybrid precoders to achieve ubiquitous low-latency mmWave communications in Industry 4.0 settings. We proposed a scheme based on alternate optimization, semidefinite relaxation and Cholesky matrix factorization to design the hybrid precoder. Also, we presented a novel scheduling formulation that takes into account the number of RF chains at the transmitter while minimizes the number of scheduling windows and channel correlation among the co-scheduled receivers. We corroborated through simulations that in terms of SINR the hybrid precoder can attain outstanding performance with a few number of RF chains. In terms of latency performance, the proposed HYDRAWAVE is capable of remaining within 9.5% of the optimal XHAUS while exhibiting noticeable advantage over SING and RAND.

APPENDIX A DERIVATION OF PROPOSITION 1

Let $C_k^* = C_k |_{\mathcal{V}_{t'}, \mathbf{F}_{t'}, \mathbf{M}_{t'}, \mathbf{w}_k}$, $\text{SINR}_k^* = \text{SINR}_k |_{\mathcal{V}_{t'}, \mathbf{F}_{t'}, \mathbf{M}_{t'}, \mathbf{w}_k}$ and $\xi_{t'}^* = \xi_{t'} |_{\mathcal{U}_{t'}, \mathbf{F}_{t'}, \mathbf{M}_{t'}, \{\mathbf{w}_k\}_{k \in \mathcal{U}_{t'}}$. From (4), the transmission latency $\xi_{t'}^*$ with known $\mathcal{U}_{t'}, \mathbf{F}_{t'}, \mathbf{M}_{t'}, \{\mathbf{w}_k\}_{k \in \mathcal{U}_{t'}}$ is defined as

$$\xi_{t'}^* = \max_{k \in \mathcal{U}_{t'}} \left\{ \frac{B_k}{\min\{C_k^*, C_{\text{max}}\}} \right\} \quad (\text{A.1a})$$

$$= \max_{k \in \mathcal{U}_{t'}} \left\{ \max \left\{ \frac{B_k}{C_k^*}, \frac{B_k}{C_{\text{max}}} \right\} \right\} \quad (\text{A.1b})$$

$$= \frac{1}{\min_{k \in \mathcal{U}_{t'}} \left\{ \min \left\{ \frac{C_k^*}{B_k}, \frac{C_{\text{max}}}{B_k} \right\} \right\}} \quad (\text{A.1c})$$

$$= \frac{1}{\min_{k \in \mathcal{U}_{t'}} \left\{ \frac{\log_2(1 + \beta \cdot \text{SINR}_k^*)}{B_k}, \frac{C_{\text{max}}}{B_k} \right\}} \quad (\text{A.1d})$$

$$= \frac{1}{\log_2 \left(\min_{k \in \mathcal{U}_{t'}} \left\{ (1 + \beta \cdot \text{SINR}_k^*)^{\frac{1}{B_k}}, 2^{\frac{C_{\text{max}}}{B_k}} \right\} \right)} \quad (\text{A.1e})$$

Because (A.1c) involves extremizations of the same type, they can be combined. When $|\mathcal{V}_t| > 1$, in general $1 + \beta \cdot \text{SINR}_k^* \leq 2^{C_{\text{max}}}$, due to interference and restricted transmit/receive power. Further, since $\log_2(\cdot)$ is monotonically increasing, then,

$$\xi_{t'}^* \approx^{-1} \min_{k \in \mathcal{U}_{t'}} \left\{ (1 + \beta \cdot \text{SINR}_k^*)^{\frac{1}{B_k}} \right\}. \quad (\text{A.2})$$

APPENDIX B DERIVATION OF PROPOSITION 2

Let $\xi_{t'}^* = \xi_{t'} |_{\mathcal{U}_{t'}}$ and $\text{SINR}_k^* = \text{SINR}_k |_{\mathcal{U}_{t'}}$ represent the latency during window t' and the SINR of receiver $k \in \mathcal{U}_{t'}$, respectively when solely \mathcal{U}_t is known. Thus, $\mathbf{F}_{t'}, \mathbf{M}_{t'}, \{\mathbf{w}_k\}_{k \in \mathcal{U}_{t'}}$ are designed in order to minimize (A.1c), i.e.,

$$\min_{\substack{\mathbf{F}_{t'} \in \Omega_F, \mathbf{M}_{t'} \in \Omega_M \\ \{\mathbf{w}_k\}_{k \in \mathcal{U}_{t'}} \in \Omega_W}} \frac{1}{\min_{k \in \mathcal{U}_{t'}} \left\{ \min \left\{ \frac{C_k^*}{B_k}, \frac{C_{\text{max}}}{B_k} \right\} \right\}}, \quad (\text{B.1})$$

which is equivalent to

$$\stackrel{(\text{B.1})}{=} \max_{\substack{\mathbf{F}_{t'} \in \Omega_F, \mathbf{M}_{t'} \in \Omega_M \\ \{\mathbf{w}_k\}_{k \in \mathcal{U}_{t'}} \in \Omega_W}} \min_{k \in \mathcal{U}_{t'}} \left\{ \min \left\{ \frac{C_k^*}{B_k}, \frac{C_{\text{max}}}{B_k} \right\} \right\} \quad (\text{B.2a})$$

$$\stackrel{(\text{B.1})}{=} \max_{\substack{\mathbf{F}_{t'} \in \Omega_F, \mathbf{M}_{t'} \in \Omega_M \\ \{\mathbf{w}_k\}_{k \in \mathcal{U}_{t'}} \in \Omega_W}} \min_{k \in \mathcal{U}_{t'}} \left\{ \frac{C_k^*}{B_k} \right\} \quad (\text{B.2b})$$

$$\stackrel{(\text{B.1})}{=} \max_{\substack{\mathbf{F}_{t'} \in \Omega_F, \mathbf{M}_{t'} \in \Omega_M \\ \{\mathbf{w}_k\}_{k \in \mathcal{U}_{t'}} \in \Omega_W}} \min_{k \in \mathcal{U}_{t'}} \left\{ \frac{\log_2(1 + \beta \cdot \text{SINR}_k^*)}{B_k} \right\} \quad (\text{B.2c})$$

$$\stackrel{(\text{B.1})}{=} \max_{\substack{\mathbf{F}_{t'} \in \Omega_F, \mathbf{M}_{t'} \in \Omega_M \\ \{\mathbf{w}_k\}_{k \in \mathcal{U}_{t'}} \in \Omega_W}} \min_{k \in \mathcal{U}_{t'}} \left\{ \frac{\text{SINR}_k^*}{B_k} \right\} \quad (\text{B.2d})$$

$$\stackrel{(B.1)}{=} \max_{\substack{\mathbf{F}_{t'}, \mathbf{M}_{t'} \in \Omega_M \\ \{\mathbf{w}_k\}_{k \in \mathcal{U}_{t'}} \in \Omega_W}} \min_{i \in \mathcal{V}_{t'}} \min_{k \in \mathcal{G}_i} \left\{ \frac{\text{SINR}_k^*}{B_k} \right\}, \quad (\text{B.2e})$$

where (B.2a) collapses to (B.2b) because C_{\max} does not depend on $\mathbf{F}_{t'}, \mathbf{M}_{t'}, \{\mathbf{w}_k\}_{k \in \mathcal{U}_{t'}}$. In (B.2c), since $\log_2(1 + \beta \cdot \text{SINR}_k^*)$ is an injective mapping of SINR_k^* , it is equivalent to (B.2d). Further, (B.2e) is an alternative notation for (B.2d).

REFERENCES

- [1] B. Martinez, C. Cano, and X. Vilajosana, "A Square Peg in a Round Hole: The Complex Path for Wireless in the Manufacturing Industry," *IEEE Communications Magazine*, vol. 57, no. 4, pp. 109–115, Apr. 2019.
- [2] A. Loch, C. Cano, G. H. Sim, A. Asadi, and X. Vilajosana, "A Channel Measurement Campaign for mmWave Communication in Industrial Settings," *CoRR*, vol. abs/1903.10502, 2019. [Online]. Available: <http://arxiv.org/abs/1903.10502>
- [3] X. Song, T. Kühne, and G. Caire, "Fully-Connected vs. Sub-Connected Hybrid Precoding Architectures for mmWave MU-MIMO," *CoRR*, Nov. 2019. [Online]. Available: <https://arxiv.org/pdf/1904.10276.pdf>
- [4] D. Zhang, Y. Wang, X. Li, and W. Xiang, "Hybridly Connected Structure for Hybrid Beamforming in mmWave Massive MIMO Systems," *IEEE Transactions on Communications*, vol. 66, no. 2, pp. 662–674, Feb. 2018.
- [5] A. Alkhateeb, O. E. Ayach, G. Leus, and R. W. Heath, "Channel Estimation and Hybrid Precoding for Millimeter Wave Cellular Systems," *IEEE Journal of Selected Topics in Signal Processing*, vol. 8, no. 5, pp. 831–846, Oct. 2014.
- [6] Z. Marzi, D. Ramasamy, and U. Madhow, "Compressive Channel Estimation and Tracking for Large Arrays in mm-Wave Picocells," *IEEE Journal of Selected Topics in Signal Processing*, vol. 10, no. 3, pp. 514–527, Apr. 2016.
- [7] H. Zhang, Y. Jiang, K. Sundaresan, S. Rangarajan, and B. Zhao, "Wireless Multicast Scheduling With Switched Beamforming Antennas," *IEEE/ACM Transactions on Networking*, vol. 20, no. 5, pp. 1595–1607, Oct. 2012.
- [8] K. Sundaresan, K. Ramachandran, and S. Rangarajan, "Optimal Beam Scheduling for Multicasting in Wireless Networks," in *ACM Mobicom*, 2009, pp. 205–216.
- [9] G. H. Sim and J. Widmer, "Finite Horizon Opportunistic Multicast Beamforming," *IEEE Transactions on Wireless Communications*, vol. 16, no. 3, pp. 1452–1465, Mar. 2017.
- [10] N. D. Sidiropoulos, T. N. Davidson, and Z. Luo, "Transmit Beamforming for Physical-Layer Multicasting," *IEEE Transactions on Signal Processing*, vol. 54, no. 6, pp. 2239–2251, Jun. 2006.
- [11] L. Tran, M. F. Hanif, and M. Juntti, "A Conic Quadratic Programming Approach to Physical Layer Multicasting for Large-Scale Antenna Arrays," *IEEE Signal Processing Letters*, vol. 21, no. 1, pp. 114–117, Jan. 2014.
- [12] J. Choi, "Iterative Methods for Physical-Layer Multicast Beamforming," *IEEE Transactions on Wireless Communications*, vol. 14, no. 9, pp. 5185–5196, Sept. 2015.
- [13] M. Bengtsson and B. Ottersten, "Optimal and Suboptimal Transmit Beamforming," in *Handbook of Antennas in Wireless Communications*, L. C. Godara, Ed., CRC Press, Aug. 2001, ch. 18.
- [14] B. Gopalakrishnan and N. D. Sidiropoulos, "High Performance Adaptive Algorithms for Single-Group Multicast Beamforming," *IEEE Transactions on Signal Processing*, vol. 63, no. 16, pp. 4373–4384, Aug. 2015.
- [15] M. Dai and B. Clerckx, "Hybrid Precoding for Physical Layer Multicasting," *IEEE Communications Letters*, vol. 20, no. 2, pp. 228–231, Feb. 2016.
- [16] E. Aryafar, M. A. Khojastepour, K. Sundaresan, S. Rangarajan, and E. Knightly, "ADAM: An Adaptive Beamforming System for Multicasting in Wireless LANs," *IEEE/ACM Transactions on Networking*, vol. 21, no. 5, pp. 1595–1608, Oct. 2013.
- [17] L. Zhou, Z. Xu, W. Jiang, and W. Luo, "Joint Multicast Beamforming and User Scheduling in Large-scale Antenna Systems," *IET Communications*, vol. 12, no. 11, pp. 1307–1314, Jul. 2018.
- [18] E. Karipidis, N. D. Sidiropoulos, and Z. Q. Luo, "Transmit Beamforming of Multiple Co-Channel Multicast Group," in *IEEE CAMSAP*, Dec. 2005, pp. 109–112.
- [19] N. Bornhorst and M. Pesavento, "An Iterative Convex Approximation Approach for Transmit Beamforming in Multi-Group Multicasting," in *IEEE SPAWC*, Jun. 2011, pp. 426–430.
- [20] O. T. Demir and T. E. Tuncer, "Multi-group Multicast Beamforming for Simultaneous Wireless Information and Power Transfer," in *EUSIPCO*, Aug. 2015, pp. 1356–1360.
- [21] E. Karipidis, N. D. Sidiropoulos, and Z. Luo, "Quality of Service and Max-Min Fair Transmit Beamforming to Multiple Cochannel Multicast Groups," *IEEE Transactions on Signal Processing*, vol. 56, no. 3, pp. 1268–1279, Mar. 2008.
- [22] Y. Gao and M. Schubert, "Group-oriented Beamforming for Multi-stream Multicasting based on Quality-of-service Requirements," in *IEEE CAMSAP*, Dec. 2005, pp. 193–196.
- [23] A. Schad and M. Pesavento, "Max-min Fair Transmit Beamforming for Multi-Group Multicasting," in *WSA*, Mar. 2012, pp. 115–118.
- [24] D. Christopoulos, S. Chatzinotas, and B. Ottersten, "Weighted Fair Multicast Multigroup Beamforming Under Per-antenna Power Constraints," *IEEE Transactions on Signal Processing*, vol. 62, no. 19, pp. 5132–5142, Oct. 2014.
- [25] M. Sadeghi, E. Björnson, E. G. Larsson, C. Yuen, and T. L. Marzetta, "Max-Min Fair Transmit Precoding for Multi-Group Multicasting in Massive MIMO," *IEEE Transactions on Wireless Communications*, vol. 17, no. 2, pp. 1358–1373, Feb. 2018.
- [26] J. Huang, Z. Cheng, E. Chen, and M. Tao, "Low-Complexity Hybrid Analog/Digital Beamforming for Multicast Transmission in mmWave Systems," in *IEEE ICC*, May. 2017, pp. 1–6.
- [27] O. T. Demir and T. E. Tuncer, "Antenna Selection and Hybrid Beamforming for Simultaneous Wireless Information and Power Transfer in Multi-Group Multicasting Systems," *IEEE Transactions on Wireless Communications*, vol. 15, no. 10, pp. 6948–6962, Oct. 2016.
- [28] M. Sadeghi, L. Sanguinetti, and C. Yuen, "Hybrid Precoding for Multi-Group Physical Layer Multicasting," in *EW*, May. 2018, pp. 1–6.
- [29] D. Christopoulos, S. Chatzinotas, and B. Ottersten, "Multicast Multigroup Precoding and User Scheduling for Frame-Based Satellite Communications," *IEEE Transactions on Wireless Communications*, vol. 14, no. 9, pp. 4695–4707, Sept. 2015.
- [30] M. R. Akdeniz, Y. Liu, M. K. Samimi, S. Sun, S. Rangan, T. S. Rappaport, and E. Erkip, "Millimeter Wave Channel Modeling and Cellular Capacity Evaluation," *IEEE Journal on Selected Areas in Communications*, vol. 32, no. 6, pp. 1164–1179, Jun. 2014.
- [31] I. Csiszár and G. Tusnády, "Information Geometry and Alternating Minimization Procedures," *Statistics & Decisions: Supplement Issues*, vol. 1, pp. 205–237, 1984.
- [32] A. Wiesel, Y. C. Eldar, and S. Shamai, "Linear Precoding via Conic Optimization for Fixed MIMO Receivers," *IEEE Transactions on Signal Processing*, vol. 54, no. 1, pp. 161–176, Jan. 2006.
- [33] Z. P. Yang and X. X. Feng, "A Note on the Trace Inequality for Products of Hermitian Matrix Power," *Journal of Inequalities in Pure and Applied Mathematics*, vol. 3, no. 5, Jul. 2002.
- [34] W. K. Ma, P. C. Ching, and Z. Ding, "Semidefinite Relaxation Based Multiuser Detection for M-Ary PSK Multiuser Systems," *IEEE Transactions on Signal Processing*, vol. 52, no. 10, pp. 2862–2872, Oct. 2004.
- [35] Z. Luo, N. D. Sidiropoulos, P. Tseng, and S. Zhang, "Approximation Bounds for Quadratic Optimization with Homogeneous Quadratic Constraints," *SIAM Journal on Optimization*, vol. 18, no. 1, pp. 1–28, Feb. 2007.
- [36] S. Zhang and Y. Huang, "Complex Quadratic Optimization and Semidefinite Programming," *SIAM Journal on Optimization*, vol. 16, no. 3, pp. 871–890, Jan. 2006.
- [37] A. A. M. Saleh and R. Valenzuela, "A Statistical Model for Indoor Multipath Propagation," *IEEE Journal on Selected Areas in Communications*, vol. 5, no. 2, pp. 128–137, Feb. 1987.
- [38] R. W. Heath, N. González-Prelcic, S. Rangan, W. Roh, and A. M. Sayeed, "An Overview of Signal Processing Techniques for Millimeter Wave MIMO Systems," *IEEE Journal of Selected Topics in Signal Processing*, vol. 10, no. 3, pp. 436–453, Apr. 2016.
- [39] X. Gao, L. Dai, S. Han, C. I. and R. W. Heath, "Energy-Efficient Hybrid Analog and Digital Precoding for MmWave MIMO Systems With Large Antenna Arrays," *IEEE Journal on Selected Areas in Communications*, vol. 34, no. 4, pp. 998–1009, Apr. 2016.
- [40] R. Méndez-Rial, C. Rusu, N. González-Prelcic, A. Alkhateeb, and R. W. Heath, "Hybrid MIMO Architectures for mmWave Communications: Phase Shifters or Switches?" *IEEE Access*, vol. 4, pp. 247–267, 2016.